Some observations of the behaviour of an adverse pressure gradient laminar boundary layer under wake impingement

Article (Published Version)

fluids

MDPI

Article

Some Observations of the Behaviour of an Adverse Pressure Gradient Laminar Boundary Layer under Wake Impingement

Vasudevan Kanjirakkad * and Thomas Irps

Thermo-Fluid Mechanics Research Centre, University of Sussex, Falmer, Sussex BN1 9QT, UK; T.Irps@sussex.ac.uk

* Correspondence: V.Kanjirakkad@sussex.ac.uk; Tel.: +44-1273678488

Abstract: The problem of laminar to turbulent transition in a boundary layer flow subjected to an adverse pressure gradient is relevant to many engineering applications. Under such conditions, the initially laminar flow within the boundary layer can undergo separation and then become turbulent upon reattachment, as transition is triggered by instabilities within the separated shear layer. In turbomachinery blades with high loading, the transition mechanism is further complicated by the presence of periodic wake disturbances shed by blades that move relatively in the upstream flow. The paper reports an experimental study of the effect of wake disturbances generated upstream on the development of a laminar boundary layer over a flat plate imposed with an adverse pressure gradient that is typical of a highly loaded front-stage compressor blade. Detailed velocity measurements using a hotwire are performed along the plate and the results are analysed both in the time domain and the frequency domain. Description of the major features identified is provided and the leading mechanisms that trigger the transition process are identified to be a possible combination of amplified Tollmien–Schlichting waves and the roll-up of vortices due to the Kelvin–Helmholtz instability of the separated shear layer.

Keywords: laminar boundary layer; adverse pressure gradient; wake disturbance; separation bubble; transition; Tollmien–Schlichting waves; Kelvin–Helmholtz instability

Citation: Kanjirakkad, V.; Irps, T. Some Observations of the Behaviour of an Adverse Pressure Gradient Laminar Boundary Layer under Wake Impingement. *Fluids* **2021**, *6*, 199. https://doi.org/10.3390/fluids6060199

Academic Editor: Mehrdad Massoudi

Received: 6 May 2021
Accepted: 21 May 2021
Published: 26 May 2021

1. Introduction

There are many engineering applications where the phenomenon of flow transition from a laminar state to a turbulent state is important and, arguably, one of the chief examples of this is turbomachinery. In gas turbine engines especially, the aerothermal performance of the compressor and turbine blades and that of the turbomachine stage itself depends on the laminar–turbulent state of the flow on the blade surfaces. On the compressor blade suction surface, the adverse pressure gradient can cause the flow to separate past the peak velocity region and this can trigger flow transition. Although turbine blade passages nominally accelerate the flow, on highly loaded turbine blades, large regions of flow diffusion could be present in the rear suction surface region, where flow separation could develop that could then initiate the transition process. On compressor and turbine blades, the transition of the boundary layer to a turbulent state causes increased losses due to the higher surface friction associated with the turbulent boundary layer [1]. In compressors, the state of the boundary layer may also have implications for their useful operating range, stall margin, stage pressure rise and performance [2]. On turbine blades, it can additionally result in higher heat transfer rates from the hot mainstream gases onto the blades, thus affecting the thermal integrity of the blades [3,4]. Besides the complicated mechanisms leading to separated boundary layer transition, the flow over the blade surfaces in turbomachines is also subjected to unsteady disturbances in the form of periodic wake impingement [5,6]. The impinged wakes are those that are generated at the trailing edge of the blades in the preceding blade row that is rotating relatively to the current. Here,

the boundary layer not only varies spatially in the streamwise direction but also temporally, thus producing a family of boundary layer profiles corresponding to different times within a wake cycle at each position along the blade. The resulting 'wake-induced transition' can substantially change the pathway leading to flow transition irrespective of whether the blade boundary layer remains attached. As the world strives to achieve a carbon-neutral economy through reduced emissions, turbomachinery designers are constantly seeking to improve turbine and compressor efficiencies and component life cycles. This often involve highly loaded compressor and turbine stages where the blade surfaces are subjected to increased adverse pressure gradient effects. It is in this context that the ability to understand, predict and control flow transition on turbomachinery blade surfaces gains renewed importance. As evident from the discussions presented in [7] summarising the NASA Minnowbrook workshop on boundary layer transition in turbomachines, the type of flow instability mechanisms that are present under typical inflow and surface pressure gradient conditions, the nature of their growth and the subsequent breakdown into fine-scale turbulence is therefore of primary importance to the developers of such applications.

Although transition under an adverse pressure gradient within a separated boundary layer has been studied by many authors, there have been fewer studies on wake-induced effects. Fewer still are those looking at the influence of a 'compressor-like wake'. Note that the flow separation of interest here is that due to the adverse pressure gradient created by the blade loading. Flow separation at the blade leading edge due to a geometry discontinuity is not discussed. A primary boundary layer instability mechanism in the form of Tollmien–Schlichting (T–S) waves has long been known [8] to be present in natural transition that usually occurs in the absence of large inflow disturbances or surface non-uniformities. Walker [9] described a correlation for the frequency of the most amplified T–S waves due to travelling disturbances. Hughes and Walker [10] noticed that T–S waves could exist in between wakes even over a compressor blade surface subjected to upstream wake impingement. Gostelow and Thomas [11] also found T–S waves to be predominant prior to separated boundary layer transition in an experimental study using a flat plate simulating a compressor blade flow under the effect of upstream-generated wakes. The authors of [11] also noted that in the presence of a highly turbulent wake (~20% wake turbulence intensity in their experimentation), the transition can advance ahead of the steady flow separation point. They described the ability of the wake-induced turbulent strip to resist the adverse pressure gradient and remain attached beyond the nominal steady flow separation point. Cumpsty et al. [12] described the importance of the calmed region following a wake patch in changing the nature of the boundary layer over a compressor blade surface. Experimental work presented by Halstead et al. [13] also notes the existence of large regions of laminar and transitional flow over the suction surface of blades in embedded compressor stages. The authors of [13] also noted the existence of calmed regions between the wake and non-wake path that have the ability to suppress flow separation and delay transition in the non-wake path. The presence of both bypass transition and separated flow transition was observed; however, the classical T–S wave-driven transition was not found to be significant. Both Halstead et al. [14] and Henderson et al. [15] discussed the effect of freestream turbulence intensity as present in a multi-stage environment on wake dispersion and how this can modify the levels of wake deficit and unsteadiness as seen by downstream blades. The latter emphasised the importance of studying blade clocking effects on transitional flow development in multistage machines and especially within embedded stages. This effect is not of interest to the present study as the focus here is on flows with relatively lower inlet turbulence levels. Hobson et al. [16] reported that, in gas turbine engines powering aircrafts, the Reynolds number of compressor blades could typically fall to 200,000 when flying at an altitude of 10,000 m. This is compared to a value of over 1 million at sea-level conditions. At such low Reynolds numbers, combined with low freestream turbulence levels (e.g., front compressor stages), separated boundary layer transition could be dominant. Low Reynolds numbers are also present in the compressors and turbines of small-core aero engines for distributed

power and boundary layer ingestion-type applications that are envisaged for efficient low-noise propulsion applications of the future.

The work presented in this paper is concerned with wake impingement and its effect on a boundary layer under an adverse pressure gradient that is undergoing transition. The chosen test case is one that is applicable to a highly loaded axial compressor blade. The paper first provides a description of the experimental setup and methodology. The effect of the propagating wake on the boundary layer is then described in the time domain using space–time (S–T) diagrams and in the frequency domain using energy spectra comparisons. A wavelet methodology is then utilised to further elucidate the frequency content of the signal within the wake path and the non-wake path.

2. Experimental Setup and Methodology

A blower-type low-speed wind tunnel is used to conduct the experiments reported in this study. The wind tunnel exit is modified to include a custom-made test section that houses a flat plate geometry with an imposed pressure profile on its surface. The test section layout is shown pictorially in Figure 1.

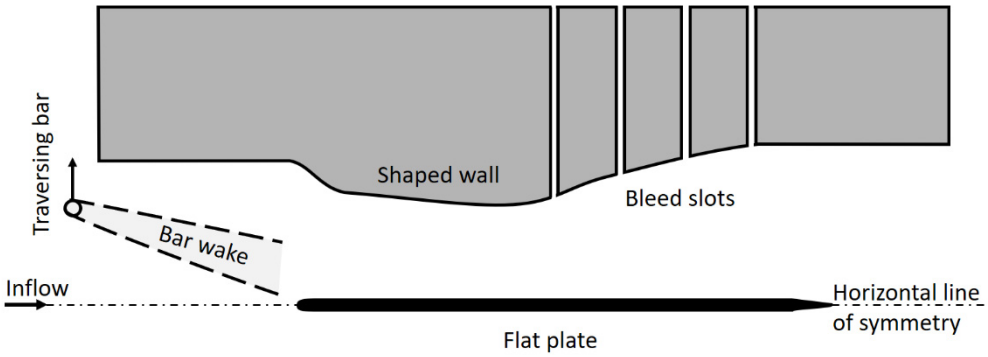

Figure 1. Schematic of the wind tunnel test section with the flat plate and the bar wake generator.

The inlet of the test section has a 456 mm square cross-section. The test plate is horizontally laid and has a thickness of 16.56 mm and is 700 mm long. The leading edge of the flat plate has a super-ellipse, as suggested by Narasimha and Prasad [17], to minimise flow separation effects on entry. Curved walls (as shown to approximate scale in Figure 1) are placed symmetrically at the top and bottom of the test section duct (i.e., above and below the test plate, respectively) in order to impose a prescribed pressure field on the plate simulating the flow over a highly loaded compressor blade. The side walls of the test section are amenable to optical measurement as they are made of acrylic. Vertical bleed slots were added downstream of the 'throat' of the shaped profile to avoid flow separation along the curved wall while trying to impose the required adverse pressure gradient along the test plate. The test plate uses a symmetric wedge at its trailing edge. An angular adjustment feature allows flow symmetry to be established at the top and bottom of the plate. The pressure field simulated in the present study is that of the highly loaded Stator 67B compressor blade, which is a geometry widely tested over the years in a large-scale linear cascade facility at the Naval Postgraduate Research Laboratory located in Monterey, California, USA (as documented by Hobson et al. [16]).

A wake disturbance generator consisting of a cylindrical bar attached to a belt that is traversed normal to the flow direction is installed at 60% plate axial chord (or 0.6 C_x) upstream of the plate leading edge. The moving belt to which a 12 mm diameter cylindrical bar is attached is traversed vertically upward at speed through a gap between the test section and the upstream section of the wind tunnel to which the test section is attached. Many researchers, such as Coull and Hodson [18] and Halstead et al. [13,14], used a similar arrangement to test the wake impingement effect on turbomachinery blade surfaces. For the experiments reported in this paper, the linear speed of the traversing bar was such that

it produced a flow coefficient (ratio of air velocity to bar linear speed) of 2.8. Although this is large compared to the flow coefficient value that is typical of an axial turbine or compressor, in the present investigation, it does allow for understanding the interaction of an 'isolated' wake with the prevailing boundary layer without being contaminated by the subsequent wake arrival prior to the recovery of the boundary layer state. The frequency of the bar wake arrival was also set low at 0.15 Hz.

The tests reported here were conducted with an inlet freestream turbulence level of 0.75%. The turbulence intensity and velocity deficit of the upstream generated wake as measured at a streamwise distance of 0.1 C_x upstream of the leading edge were 12% and 22%, respectively. These are comparable to the values reported in the studies by Halstead et al. [13,14] and that by Camp and Shin [19], who conducted wake measurements in single and multi-stage compressor facilities. The inlet velocities were monitored using a pitot-wall static arrangement at two streamwise locations: one upstream of the test section gap (used for bar passing) and a second one downstream of this gap. The wall static pressure values above and below the plate were also monitored downstream of the plate trailing edge to ensure flow symmetry.

The imposed pressure gradient distribution simulating that over the suction side of the Stator 67B compressor blade is verified using a number of streamwise surface static pressure tappings that the top surface of the test plate was instrumented with. These were slightly offset from the centreline of the plate in order to enable velocity measurements such as those using a constant temperature hotwire anemometer (CTA) probe or particle image velocimetry (PIV) along the true centreline. A custom-built array of $\pm$2000 Pa range transducers were employed for the steady pressure measurements. The measured non-dimensional surface static pressure (C_p) profile that resulted, at a plate axial chord-based Reynolds number of 210,000, is compared against that of the Stator 67B in Figure 2. The start and the end of the prevailing separated zone on the plate surface have been shown annotated by the letters S and R, respectively, and the separated region is also highlighted by the shaded green region. The locations S and R correspond to a streamwise distance of approximately 0.48 C_x and 0.68 C_x downstream of the plate leading edge, respectively. The shaped walls of the test section as mentioned above were designed to match the C_p distribution of the Stator 67B blade for its design condition at a much higher Reynolds number of 640,000. However, the test section has managed to capture the separation bubble formation and the flow diffusion correctly at the reduced Reynolds number of 210,000. A slight discrepancy between the C_p values obtained from the cascade [16] and the present data is seen over the separated region. Although the cause of this difference is not known, a similar difference was also observed in the large eddy simulation-based numerical study conducted by Rizvi and Mathew [20]. The location and the length of the separation bubble, however, are comparable to those reported in [16].

Flow velocity measurements at selected streamwise locations along the centreline were carried out using a CTA probe. A single wire 55P15 1-D miniature boundary layer probe with a 5 µm diameter sensing wire was used in conjunction with Dantec Dynamics's (Skovlunde, Denmark) Streamline 90N10 CTA processor. The analogue output from the above unit was digitally acquired using a National Instruments supplied PXI-6363 board connected to a personal computer. All data were logged using the National Instruments (Austin, TX, USA) LabView software. The CTA signals were acquired at a sampling rate of 20 kHz and were analogue-filtered at 10 kHz as required by the Nyquist criterion for aliasing-free data sampling. Figure 3a shows a contour map of the ensemble averaged streamwise (x-direction) velocity normalised by the freestream velocity, $\langle u/u_\infty \rangle$. These data were taken without the presence of the incoming wakes, hereafter referred to as the 'steady-inlet' condition. The y-axis of both plots show the wall normal distance normalised by the plate axial chord. The approximate separation and re attachment points of the separation bubble are annotated by the letters S and R, respectively, and are consistent with the measured surface C_p profiles shown in Figure 2. Figure 3b shows the corresponding normalised streamwise velocity profiles. The laminar boundary layer that exists upstream

of the separation point becomes inflectional inside the bubble and the inflection points move away from the wall as the flow progresses downstream. The profiles beyond the reattachment point are typical of a boundary layer that is reattaching in a turbulent manner. The red line shows the locus of points where the *rms* value of the velocity, u_{rms}, is the maximum along each profile. Note that the locations of the maximum fluctuations lie very close to the inflection points in each of the velocity profiles shown. Diwan and Ramesh [21], who made a similar observation, stated that this is due to the enhancement of the transfer of energy from the mean flow to the fluctuations by the shear present along the points of inflection. The u_{rms} intensity contours are plotted in Figure 4, with the red line representing the locus of maximum u_{rms} values overlaid on top. The data presented show the growth of the fluctuations along the regions of high shear layer, as noted previously. The streamwise location of the maximum u_{rms} intensity anywhere over the plate coincides with the reattachment region of the bubble, an observation which was also made by Watmuff [22] and Marxen et al. [23].

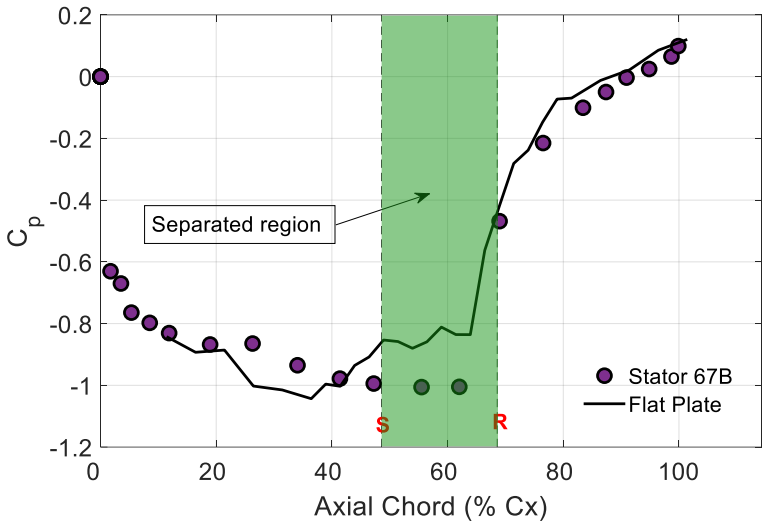

Figure 2. Measured non-dimensional surface pressure (C_p) distribution over the plate. The black line represents data from the current measurements whereas the filled symbols correspond to Stator 67B data from Hobson et al. [16]. S and R represent the approximate locations of flow separation and reattachment from the current measurements.

Table 1 provides a summary of the geometrical aspects of the test setup and the conditions related to the flow used for the study.

Table 1. Test section and inlet flow specification.

Parameter	Unit	Value
Plate length (C_x)	mm	700
Plate width	mm	456
Plate thickness	mm	16.56
Bar diameter	mm	12
Bar frequency	Hz	0.15
Wake turbulence [1]	%	12
Wake velocity deficit [1]	%	22
Flow coefficient	-	2.8
Reynolds number (Re_x)	-	210,000
Inlet free stream turbulence	%	0.75

[1] Value measured at a distance of 0.1 C_x upstream of the plate leading edge.

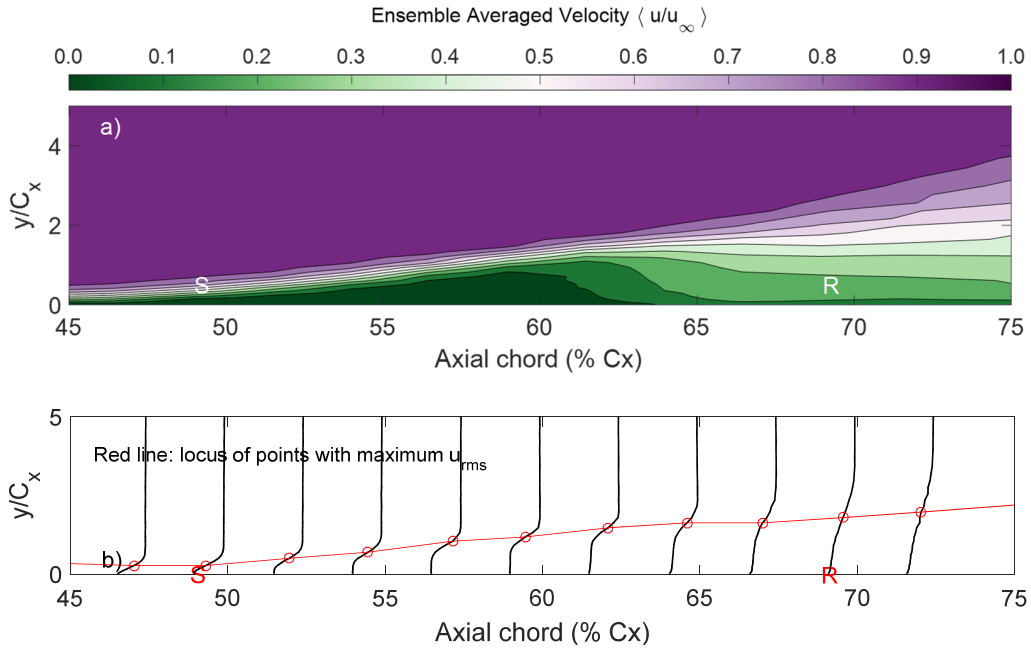

Figure 3. Averaged streamwise velocity, $\langle u/u_\infty \rangle$, measured using the CTA around the separation bubble: (**a**) contour map, (**b**) wall normal velocity profile. S and R show approximate locations of separation and reattachment, respectively. The red line is the locus of maximum u_{rms} intensity.

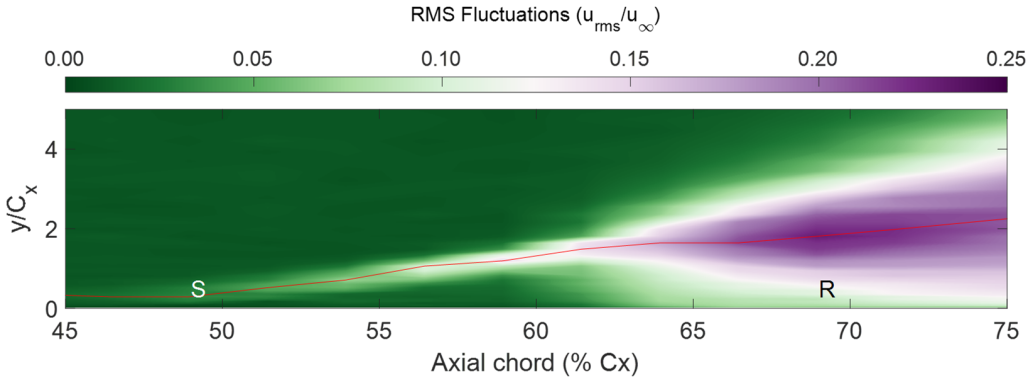

Figure 4. Contours of normalised u_{rms}. The red line is the locus of maximum u_{rms} intensity. S and R represent the approximate locations of flow separation and reattachment from the current measurements.

3. Results and Discussion

The previous section provided a description of the test setup and the features of the background flow (base flow) present in the absence of any periodic wake disturbances at the inlet. In the following section, the modification of the base flow by the introduction of the periodic bar wake (whose characteristics were described in the previous section) is discussed. As previously mentioned, all the measurements reported in this paper correspond to a plate chord-based Reynolds number of 210,000. Hotwire data are presented and discussed both in the time domain and in the frequency domain and all the signals for these are collected along the locus of maximum u_{rms} (corresponding to the steady-inlet case) as shown by the red line in Figure 3a. At each of the streamwise locations, 128 ensembles were collected with reference to a trigger signal within a wake cycle.

3.1. Time Domain Analysis

Figure 5 shows the space–time (S–T) diagram of the velocity signals acquired along the locus of the peak u_{rms}. In each of the plots shown, the x-axis shows the time in seconds and the y-axis shows the streamwise location expressed as a percentage of the plate chord. The time axis shows one second's worth of the signal and the space axis shows distances from 16% to 78% axial chord (0.16 C_x to 0.78 C_x) downstream of the plate leading edge. For comparison, the cases without (steady-inlet) and with the presence of the wake at the inlet to the test section (hereafter referred to as 'wake-inlet') are plotted side-by-side. The S–T diagrams of the raw velocity signals are presented first for the steady-inlet, in Figure 5a, and for the wake-inlet, in Figure 5d. In agreement with the C_p distribution over the surface, as shown earlier in Figure 2, the velocity can be seen to decrease past the peak suction point (located near 0.4 C_x) following the initial region of acceleration near the plate leading edge. The strong deceleration downstream of 0.4 C_x causes the laminar boundary layer (seen with relatively smooth contours) to separate around 0.49 C_x (the region annotated as S in the figure) and to reattach as a turbulent boundary layer (seen with streaky contours) around 0.69 C_x (the region annotated as R in the figure). In reality, the streaky nature of the contours starts before reattachment at around 0.6 C_x, which is slightly upstream of the peak height of the separation bubble. The instability of the shear layer is known to grow linearly over the front part of the separation bubble before becoming non-linear and triggering the formation of Kelvin–Helmholtz (K-H) vortex roll-up. This vortex roll-up enhances the process of flow breakdown into turbulence. In fact, the vortex structures ensure that high momentum fluid from the external flow is brought closer to the wall, thus enabling the separated flow to reattach back onto the surface. These observations are consistent with those of [21–23]. The main difference between the steady-inlet case in Figure 5a and the wake-inlet case in Figure 5d is the presence of the convective disturbances due to the wake that is present for the latter. The wake is not only characterised by an 'avenue' of reduced velocity but also by a region of increased fluctuations, as seen by the 'streakiness' of the contours within the wake avenue in Figure 5d. It is known [12] that the wake as it impinges on the blade surface brings forward the location within the boundary layer where turbulence is present, although this turbulence is only partially present during the wake cycle in the upstream regions and only when the foot of the wake grazes the surface where the flow is laminar.

Another major difference between the steady-inlet case and the wake-inlet case is the appearance of a region of reduced fluctuations and increased velocity behind the wake deficit. This region is annotated as C in Figure 5d–f and this corresponds to the 'calmed region'. The calmed region is a relatively thin, non-stable passage of flow following a turbulent wake (or turbulent spot), resembling a 'laminar region'. The perceived high velocities associated with region C are due to the passage of the calmed region momentarily making the boundary layer thinner and thus exposing the 'freestream' flow to the measurement probe. However, as noted in [12], it would be erroneous to associate the properties of a laminar boundary layer with the calmed region. Although resistant to fluctuations, the skin friction under the calmed region is comparable to that in a turbulent flow, making it more resistant to adverse pressure gradients. The velocity variation within the calmed region is almost linear with the wall normal distance, resembling the laminar sublayer under a turbulent boundary layer but extending all the way to the freestream. This passage of 'calmed' flow relaxes back to that of a traditional laminar boundary layer after sufficient time. Figure 5b,e essentially show the same data as in Figure 5a,d but in the ensemble averaged form and thus the random fluctuations due to the disturbances are no longer visible. This clearly shows the separated region and its suppression partly during the time interval due to the arrival of the calmed region. In Figure 5c,f, the evolution of the wake disturbance alone is isolated by subtracting the mean steady flow velocity field. This makes the contours of the velocity field due to the steady-inlet look uniform throughout, whereas that due to the wake-inlet shows the effect of the wake propagation alone.

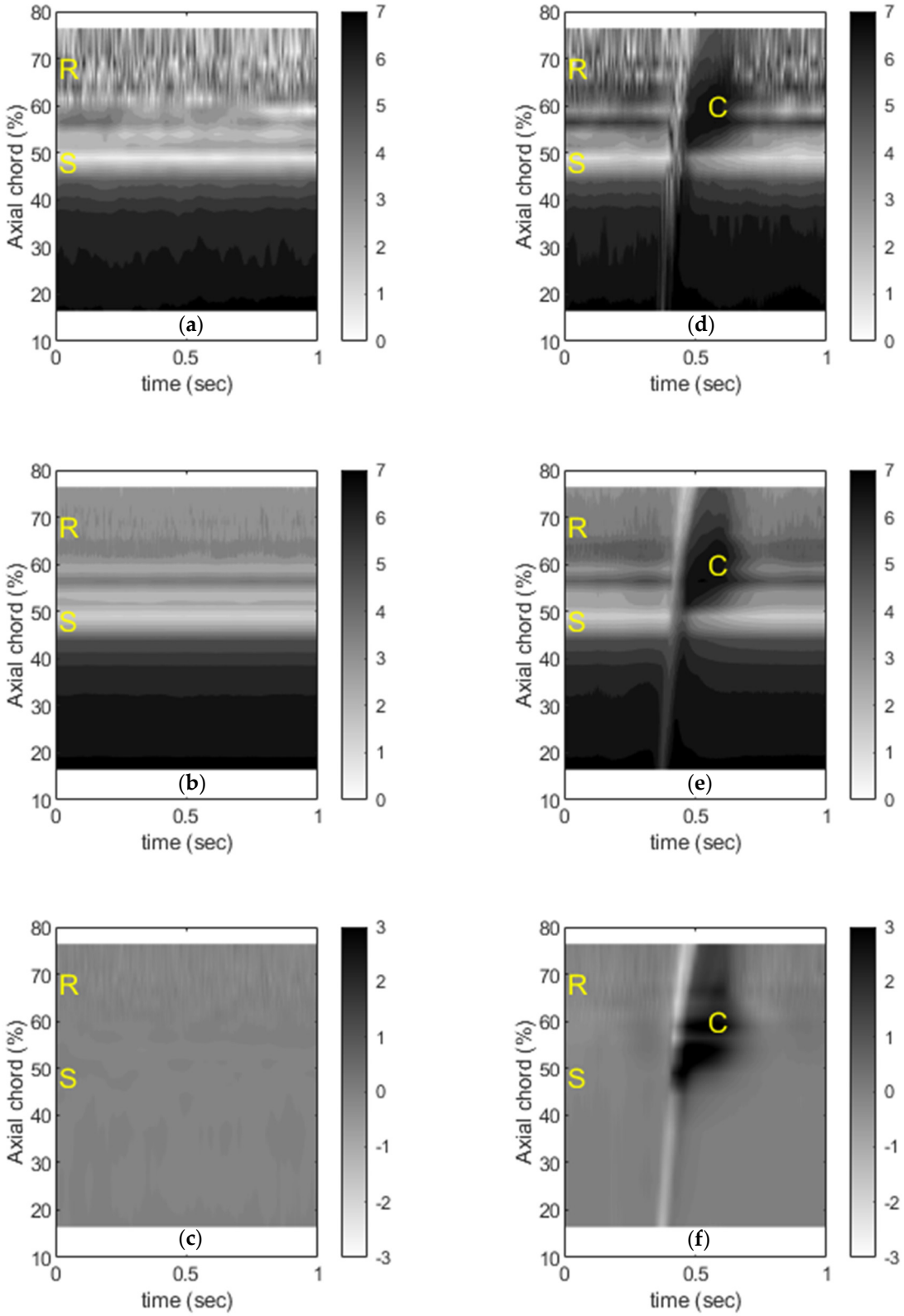

Figure 5. S–T diagram of hotwire signals acquired along the locus of peak u_{rms}. Raw signals are shown first for (**a**) steady-inlet and (**b**) wake-inlet. Ensemble averaged signals are presented next for (**c**) steady-inlet and (**d**) wake-inlet. Finally, the ensemble averaged effect due to the disturbances alone is shown by subtracting the mean steady flow for (**e**) steady-inlet and (**f**) wake-inlet. S and R represent the approximate locations of flow separation and reattachment from the current measurements. C represents the 'calmed region'.

More insight into the velocity field is available by plotting the individual velocity signals along the streamwise positions as shown in Figure 6. For the steady-inlet case (Figure 6a), the velocity field remains undisturbed and laminar until the separation point (~0.49 C_x). The front portion of the bubble, often identified as the dead-air region [24], is known to be a region of very low amplitude disturbances and linear evolution of disturbance is expected [21]. As seen in Figure 6a, the front part of the bubble (0.49 C_x to 0.55 C_x) is free from disturbances, although a low-frequency, low-amplitude, wavy structure seems to appear and grow towards the rear part of this region. However, by 0.59 C_x, another relatively higher-frequency periodic structure is visible, which seems to grow rather rapidly before becoming unrecognisable due to the flow breakdown in the rear part of the bubble. A similar behaviour was observed by Diwan and Ramesh [21], who identified that the growth of the disturbances could be broadly divided into to the mild-growth and small dispersion region before the separation point, a region of exponential growth from the front of the bubble to the peak height of the bubble and finally a region of nonlinear breakdown downstream of the peak bubble. The peak height of the bubble in the present measurement is located around 0.62 C_x downstream of the plate leading edge.

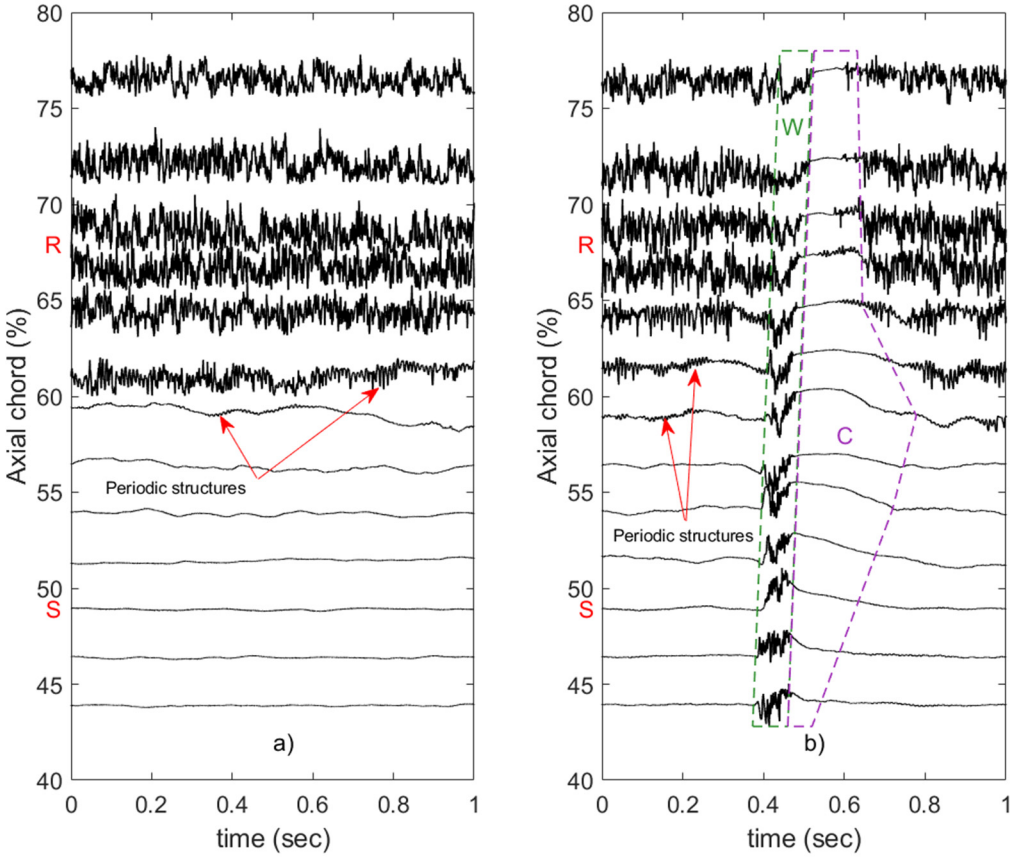

Figure 6. Development of the time series of the velocity signals with distance for (**a**) steady-inlet and (**b**) wake-inlet. S and R represent the approximate locations of flow separation and reattachment from the current measurements.

For the wake-inlet case, as shown in Figure 6b, the above observations from the stead-inlet case largely remain true. Two important differences are the additional features that exist within the wake disturbance itself (annotated by the letter W and enclosed within the green boxed region) and the calmed region that trails the wake disturbance (annotated by the letter C and demarcated by the purple boxed region). The convective wake disturbance is clearly identifiable in the upstream laminar boundary layer regions as a highly turbulent patch. One intriguing observation is that the diffusion (in the sense of temporal stretching

of the signal) of the wake seems to be lower compared to that reported for a loudspeaker-generated wave packet in [21]. This is despite similar levels of diffusion being present in the current study and that reported in [21]. The calmed region was already visible, as described in Figure 5, for the regions over the bubble; however, the time series of the signals indicate the presence of it even in the regions upstream of the bubble, which is less recognisable in the nominal laminar flow with a higher freestream velocity. As noted before, the calmed region is characterised by a thin boundary layer, its resistance to turbulent fluctuations and its ability to resist separation on the account of higher skin friction. The calmed region is seen to undergo dispersion (stretching) within the nominally laminar flow upstream and in the front portion of the boundary layer. However, as the disturbances grow towards the peak of the bubble and as the flow breaks down further downstream, the extent of the calming effect shrinks. There is also some evidence that some disturbances can penetrate into the calmed region downstream of the peak bubble height region. These disturbances seem to be of the periodic type, as noted earlier in the section, rather than the random fluctuation associated with turbulence. This aspect should become much clearer if one were to do a frequency domain analysis of the above signals. It may also help to elucidate the origins of the periodic structure that was noted upstream of the location of the peak bubble height.

3.2. Frequency Domain Analysis

The power spectra associated with the velocity signals seen in Figure 6 are presented. Figure 7 shows the spectra for both the steady-inlet and the wake-inlet cases with the same plot legend applicable to both. In general, the energy associated with the fluctuations increases as they grow with distance away from the leading edge. At any given streamwise location prior to the location of peak bubble height (0.62 C_x), the wake-inlet signals have several orders of magnitude more energy than the steady-inlet signals. This is true across the entire frequency spectrum that is plotted and can be attributed to the energy of the fluctuations contained within the wake (higher turbulent content with moderate to high frequencies) and that associated with the velocity deficit within the wake (lower frequencies). The inertial subrange containing the Taylor micro-scale is usually associated with the $-5/3$rd power and is shown alongside the spectra in the plots (black solid line). It is apparent that the flow conforms to this regime post reattachment (0.62 C_x) for the steady-inlet as well as the wake-inlet cases. A dominant feature of the spectra for both cases is the existence of a narrow frequency hump peaking at a frequency of 100 Hz (and its higher harmonics). It is notable that the energy contained in the hump becomes less dominant after reattachment, suggesting a break-up of flow producing turbulent structure in the inertial subrange. In other words, the inertial subrange only starts post-reattachment.

With several of the authors mentioned earlier [9–11,13–15] pointing to the possibility of the existence and dominance of amplified T–S waves and others (e.g., [21]) observing the opposite, there is some interest in ascertaining the source of this frequency hump. Walker [9] described a correlation for the most amplified T–S wave frequencies as a function of the displacement thickness-based Reynolds number (Re_{δ^*}), boundary layer edge velocity (U_{edge}) and kinematic viscosity (ν) of the form,

$$f_{TS} = 3.2\frac{U_{edge}^2 {Re_{\delta^*}}^{-3/2}}{2\pi\nu} \quad (1)$$

This was evaluated using the time-averaged velocity profiles for the steady-inlet case and the results are plotted in Figure 8. The dominant frequency (f_{TS}) is represented in Hz as well as in the circular frequency ($2\pi f_{TS}$) form. The values for f_{TS} immediately upstream and downstream of the separation bubble are approximately 45 Hz (circular frequency ~300 rad/s) and 5 Hz (circular frequency of ~30 rad/s), respectively. However, prior to the bubble, f_{TS} decreases almost linearly from 160 Hz at a distance of 0.16 C_x downstream of the plate leading edge until the front of the separation bubble. Figure 8 tells us that a T–S wave with a frequency of 100 Hz could well be formed in the streamwise

region close to 0.40 C_x. These T–S disturbances could then become amplified in the free shear layer over the separation bubble as the latter is widely known to amplify upstream disturbances exponentially [25]. The T–S waves and their frequencies, if present, may be predicted by linear stability theory and this requires obtaining the eigenvalues of the Orr–Sommerfeld equation. Such an analysis is currently not available for the present work. Since measurements using a single-wire CTA probe, as reported in this study, cannot resolve negative velocities that may be present within regions of the separation bubble with an inflectional profile, a *tanh*-based curve was fitted through the profiles (Dovgal et al. [26]). This, however, only had a marginal effect on the T–S frequencies, as predicted by Equation (1).

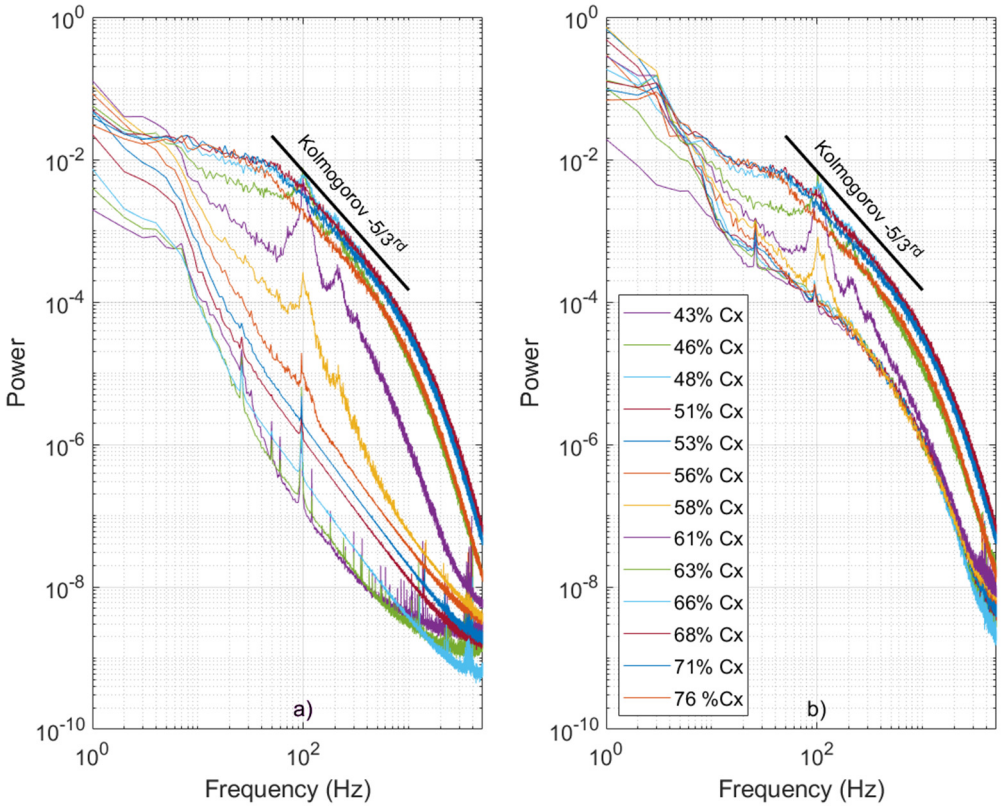

Figure 7. Power spectra calculated from hotwire velocity signals for (**a**) steady-inlet and (**b**) wake-inlet.

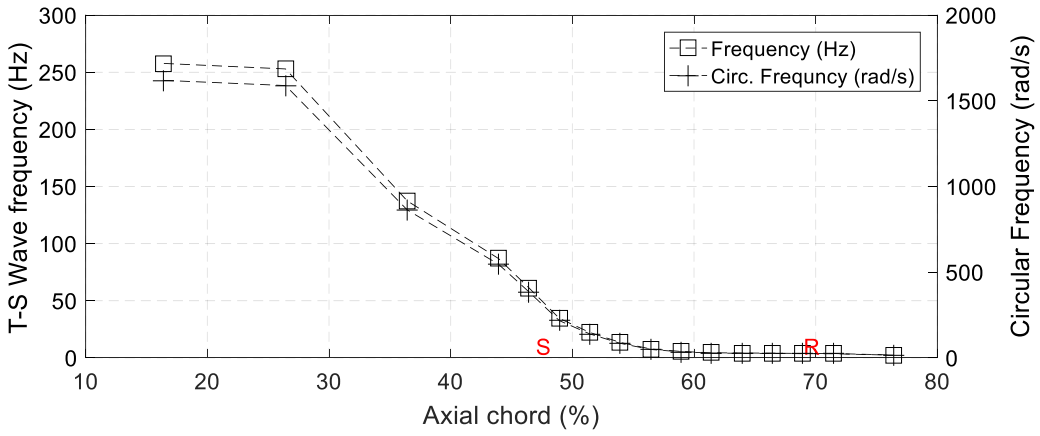

Figure 8. Most amplified T–S wave frequencies calculated using the correlation found in [9]. S and R represent the approximate locations of flow separation and reattachment from the current measurements.

Another phenomenon that could be the cause of the said frequency hump is the shear layer roll-up above the separation bubble that is known to occur due to the K–H instability. As noted by Simoni et al. [27], the K–H instability is influenced by the adverse pressure gradient and flow velocity at separation (linked to the blade loading) and the vortex shedding frequency is influenced by the shear layer thickness. The above authors proposed an expression for the Strouhal number associated with the K–H instability as a function of the non-dimensional streamwise velocity (u^*), the streamwise velocity gradient ($\partial u^*/\partial s^*$) and the exit velocity-based Reynolds number (Re_2) of the form,

$$St = \left(\frac{1}{c_2} Re_2 \frac{\partial u^*}{\partial s^*} u^{*2} \right)^{0.5}, \quad (2)$$

where c_2 is a constant. The authors of [27] showed that for Reynolds numbers less than 300,000, the Strouhal number predicted by Equation (2) is within ±15% of the experimentally observed values for the test cases that they considered. For the present study, the Strouhal numbers evaluated in this manner corresponded to a frequency of 110 Hz near the peak height of the bubble and 95 Hz immediately downstream of the averaged bubble reattachment point. These numbers are extremely close to the experimentally observed frequency hump at 100 Hz and point to the dominance of K–H instability in this region.

The correlation-based analyses presented above and the proximity of the predicted frequencies to the experimentally observed frequency hump suggest a strong possibility of the existence of either phenomena. In other words, the origin of the frequency hump could be either the amplification of T–S waves (that originate in the close to 0.4 C_x downstream of the plate leading edge) or the shear layer instability of the K–H type over the separation bubble. In the time series data presented in Figure 6, periodic structures are visible at least as early as 0.59 C_x.

Stieger and Hodson [28] used a wavelet-based analysis of hot-film signals to reveal the presence of T–S waves when studying the wake-induced transition over a separated boundary layer on a flat plate. The above authors concluded that this highlighted the existence of natural transition phenomena between wake passing events. As in [28], the current velocity signal data were also analysed using a Morlet wavelet ($\omega_0 = 6$) transform. The reason for selecting the Morlet wavelet is its resemblance to the wave packets found in the measured flow. Hughes and Walaker [10] also used a Morlet wavelet for analysing their experimental data. As noted in [10], the wavelet analysis helps with the identification of wave packets (with a specific frequency) that appear randomly in time under the influence of free-stream turbulence. Figure 9 shows the contours of wavelet power corresponding to the location 0.59 C_x downstream of the plate leading edge for both the steady-inlet and the wake-inlet cases. For the contours in each case, the corresponding velocity time series is shown above the contour map. Time is shown along the horizontal axis and frequency along the vertical logarithmic axis (base 2). The contour levels are also in the logarithmic scale (base 2). The black line is the 95% confidence enclosure. The advantage of the wavelet power spectrum as plotted in the above manner is that it combines both time and frequency information in one plot. It therefore makes it easier to understand the frequencies that are present at different instances within a given signal. For example, Figure 9a allows us to identify, along its vertical axis, the most dominant frequency (100 Hz) corresponding to the frequency hump in the power spectrum that was presented earlier in Figure 7. A horizontal red (dashed) line in Figure 9a now signifies this dominant frequency. It is clear that, for the steady-inlet case, the velocity signal has a distinct 100 Hz spectral content at this location all along its length, with islands of highs (purple) and lows (green), pointing to the possibility that these could indeed be the amplified T–S waves that were potentially generated at a location close to 0.40 C_x downstream of the plate leading edge. For the wake-inlet case, the wavelet power spectrum contours show a distinct region corresponding to the wake disturbance, which has fluctuations present within it in the full range of frequencies shown. Interestingly, the there are two distinct peaks visible within the wake corresponding to the frequency of 100 Hz. As in the steady-inlet case, fluctuations at 100 Hz are present all along

the signal, except in the time gap of 0.5 s to 0.7 s, which can be identified as the calmed region. Therefore, if T–S wave amplification is indeed the cause of the 100 Hz spectral content at this location, then the wave is clearly damped within the calmed region.

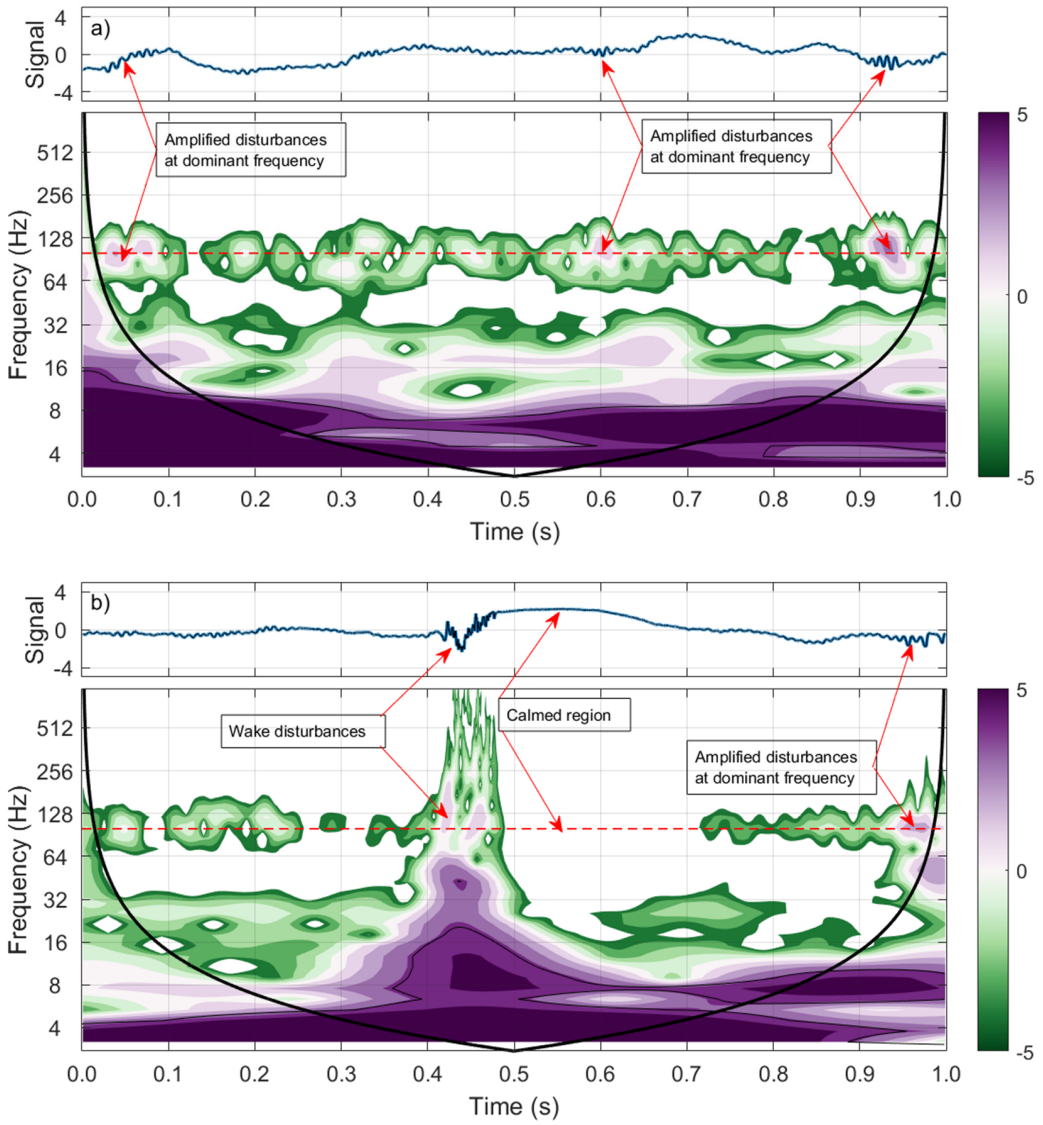

Figure 9. Wavelet transform contours for (**a**) steady-inlet and (**b**) wake-inlet. The dashed red line represents the dominant frequency in the frequency hump (100 Hz).

Although not shown in the paper, for both steady- and wake-inlet cases, the wavelet power contours show that the amplitude of the 100 Hz fluctuations peaks close to the maximum bubble height location (0.62 C_x), beyond which its distinctiveness is lost as the flow starts to break down non-linearly, thus bringing the higher-frequency regions highlighted in the contour plot. While the generation of T–S waves well upstream of the bubble and their amplification is a clear possibility, as suggested by the evaluation using Equation (2), the shedding frequency of the rolled-up vortices due to K–H instability is also in the 95–110 Hz region. In fact, a direct numerical simulation (DNS) study by McAuliffe and Yaras [29] based on the results from a flat plate experimental test case has shown that both T–S and K–H instabilities can play a key role in the transition process if they occur at a similar frequency, as is the case in the present study. The above authors argued that although the K–H instability mechanism is key to the ultimate breakdown into turbulence, as it enables cross-stream mixing for the reattachment of the separated shear

layer, the amplified T–S waves contribute considerably to the cross-stream momentum exchange in the separated shear layer. Furthermore, Diwan and Ramesh [21] show evidence to modify the view that the origin of the inviscid instability in a bubble is related to the Kelvin–Helmholtz mechanism associated with the detached shear layer outside the bubble. They show that the inflectional instability associated with the separated shear layer is an extension of the instability of the upstream attached adverse pressure gradient boundary layer and the origin of the instability lies upstream of the separation bubble. They argue, further, that only when the separated shear layer has moved away sufficiently from the wall (e.g., peak height of the bubble) does the vorticity thickness-based non-dimensional frequency scale associated with K–H instability come into play and such a mode become dominant.

4. Conclusions

This paper describes experimental observations of the behaviour of a laminar boundary layer subjected to an adverse pressure gradient, similar to that which exists over a highly loaded axial compressor blade, under the influence of an upstream-generated wake. Velocity measurements using a single-wire CTA probe tracked the boundary layer development over a flat plate with the imposed adverse pressure gradient. Time domain and frequency domain interpretations are presented. The following observations are of interest.

In the absence of the upstream-generated wake (steady-inlet), the initially laminar boundary layer developed inflectional velocity profiles such that the maximum *rms* fluctuation was found close to the point of inflection. The regions of the bubble upstream of its peak height showed a distinct periodic structure in their velocity signals.

The upstream bar wakes, when introduced, convected downstream as a distinct turbulent patch that was followed by a region of higher velocity devoid of fluctuations, which was identified as the calmed region. The dispersion of the turbulent wake patch was found to be minimal. The calmed region, on the other hand, became elongated upstream of the bubble and in the front portion of the bubble, but then shrunk beyond the peak height location of the bubble. The periodic structures as seen in the steady-inlet case were also observable in the presence of the wake.

The frequency power spectrum showed the presence of a distinct frequency hump centred at 100 Hz. A velocity profile-based correlation identified the possibility that T–S waves with a similar frequency could indeed be generated in the regions upstream of the separation bubble. A separate velocity gradient-based correlation also predicted K–H instability-related shedding frequencies in an identical frequency range. For both steady and wake-inlet cases, a wavelet-based analysis clearly pointed to the existence of 100 Hz frequency content within the periodic structures that were identified in the front part of the bubble. The wavelet power contours also showed the absence of this frequency within the calmed region. It is concluded that the observed frequency hump in the power spectra is due to the combined effect of possible T–S wave amplification and the K–H instability of the separated shear layer and that this is the mechanism of the transition onset.

Author Contributions: T.I. conducted all the reported measurements under the supervision of V.K. T.I. was also responsible for preparing the raw data and their calibration post-acquisition. All the text and the figures in the paper are by V.K., who was also responsible for the final processing of the data towards obtaining the figures in the format presented. All authors have read and agreed to the published version of the manuscript.

Funding: This research was funded by the University of Sussex Research Development Fund (RDF Round 4) and the authors gratefully acknowledge the financial support provided.

Institutional Review Board Statement: Not applicable.

Informed Consent Statement: Not applicable.

Data Availability Statement: Not applicable.

Conflicts of Interest: The authors declare no conflict of interest. The funders had no role in the design of the study; in the collection, analyses, or interpretation of data; in the writing of the manuscript, or in the decision to publish the results.

References

1. Denton, J.D. The 1993 IGTI Scholar Lecture: Loss Mechanisms in Turbomachines. *ASME J. Turbomach.* **1993**, *115*, 621–656. [CrossRef]
2. Kerrebrock, J.L.; Reijnen, D.P.; Ziminsky, W.S.; Smilg, L.M. Aspirated Compressors. In Proceedings of the ASME 1997 International Gas Turbine and Aeroengine Congress and Exhibition, Orlando, FL, USA, 2–5 June 1997. [CrossRef]
3. Turner, A.B. Local Heat Transfer Measurements on a Gas Turbine Blade. *J. Mech. Eng. Sci.* **1971**, *13*, 1–12. [CrossRef]
4. Narasimha, R. The laminar-turbulent transition zone in the turbulent boundary layer. *Prog. Aerosp. Sci.* **1985**, *22*, 29–80. [CrossRef]
5. Liu, X.; Rodi, W. Experiments on transitional boundary layers with wake-induced unsteadiness. *J. Fluid Mech.* **1991**, *231*, 229–256. [CrossRef]
6. Hodson, H.P.; Howell, R.J. Bladerow interactions, transition, and high-lift aerofoils in low-pressure turbines. *Annu. Rev. Fluid Mech.* **2005**, *37*, 71–98. [CrossRef]
7. Narasimha, R. Boundary layer transition in turbomachines. *Curr. Sci.* **1998**, *74*, 274–279. Available online: http://www.jstor.org/stable/24101493 (accessed on 17 May 2020).
8. Schubauer, G.B.; Skramstad, H.K. Laminar boundary layer oscillations and the stability of laminar flow. *J. Aeronaut. Sci.* **1947**, *14*, 69–78. [CrossRef]
9. Walker, G.J. Transitional flow on axial turbomachine blading. *AIAA J.* **1989**, *27*, 595–602. [CrossRef]
10. Hughes, J.D.; Walker, G.J. Natural transition phenomena on an axial compressor blade. *ASME J. Turbomach.* **2001**, *123*, 392–401. [CrossRef]
11. Gostelow, J.P.; Thomas, R.L. Response of a Laminar Separation Bubble to an Impinging Wake. *ASME J. Turbomach.* **2005**, *127*, 35–42. [CrossRef]
12. Cumpsty, N.A.; Dong, Y.; Li, Y.S. Compressor Blade Boundary Layers in the Presence of Wakes. In Proceedings of the ASME 1995 International Gas Turbine and Aeroengine Congress and Exposition, Houston, TX, USA, 5–8 June 1995. [CrossRef]
13. Halstead, D.E.; Wisler, D.C.; Okiishi, T.H.; Walker, G.J.; Hodson, H.P.; Shin, H. Boundary Layer Development in Axial Compressors and Turbines: Part 1 of 4—Composite Picture. *ASME J. Turbomach.* **1997**, *119*, 114–127. [CrossRef]
14. Halstead, D.E.; Wisler, D.C.; Okiishi, T.H.; Walker, G.J.; Hodson, H.P.; Shin, H. Boundary Layer Development in Axial Compressors and Turbines: Part 2 of 4—Compressors. *ASME J. Turbomach.* **1997**, *119*, 426–444. [CrossRef]
15. Henderson, A.D.; Walker, G.J.; Hughes, J.D. The Influence of Turbulence on Wake Dispersion and Blade Row Interaction in an Axial Compressor. *ASME J. Turbomach.* **2006**, *128*, 150–157. [CrossRef]
16. Hobson, G.V.; Hansen, D.J.; Schnorenberg, D.G.; Grove, D.V. Effect of Reynolds Number on Separation Bubbles on Compressor Blades in Cascade. Monterey, California, Naval Postgraduate School. 1998. Available online: https://calhoun.nps.edu/handle/10945/37950 (accessed on 4 April 2013).
17. Narasimha, R.; Prasad, S.N. Leading edge shape for flat plate boundary layer studies. *Exp. Fluids* **1994**, *17*, 358–360. [CrossRef]
18. Coull, J.D.; Hodson, H.P. Unsteady boundary-layer transition in low-pressure turbines. *J. Fluid Mech.* **2011**, *681*, 370–410. [CrossRef]
19. Camp, T.R.; Shin, H. Turbulence Intensity and Length Scale Measurements in Multistage Compressors. *ASME J. Turbomach.* **1995**, *117*, 38–46. [CrossRef]
20. Rizvi, S.A.H.; Mathew, J. Large Eddy Simulation of Transitional Flow in a Compressor Cascade. In Proceedings of the ASME Turbo Expo 2017: Turbomachinery Technical Conference and Exposition, Charlotte, NC, USA, 26–30 June 2017. [CrossRef]
21. Diwan, S.S.; Ramesh, O.N. On the origin of the inflectional instability of a laminar separation bubble. *J. Fluid Mech.* **2009**, *629*, 263–298. [CrossRef]
22. Watmuff, J.H. Evolution of a wave packet into vortex loops in a laminar separation bubble. *J. Fluid Mech.* **1999**, *397*, 119–169. [CrossRef]
23. Marxen, O.; Lang, M.; Rist, U.; Wagner, S. A combined experimental/numerical study of unsteady phenomena in a laminar separation bubble. *Flow Turbul. Combust.* **2003**, *71*, 133–146. [CrossRef]
24. Gaster, M. *The Structure and Behaviour of Separation Bubbles*; ARC London R&M: London, UK, 1967.
25. Dovgal, A.V. Flow Instability in Laminar Separation Bubbles. In *Laminar-Turbulent Transition*; IUTAM Symposia (International Union of Theoretical and Applied Mechanics); Fasel, H.F., Saric, W.S., Eds.; Springer: Berlin/Heidelberg, Germany, 2000. [CrossRef]
26. Dovgal, A.V.; Kozlov, V.V.; Michalke, A. Laminar boundary layer separation: Instability and associated phenomena. *Prog. Aerosp. Sci.* **1994**, *30*, 61–94. [CrossRef]
27. Simoni, D.; Ubaldi, M.; Zunino, P. A simplified model predicting the Kelvin-Helmholtz instability frequency for laminar separated flows. *ASME J. Turbomach.* **2015**, *138*, 044501. [CrossRef]
28. Stieger, R.D.; Hodson, H.P. Unsteady dissipation measurements on a flat plate subject to wake passing. *Proc. Inst. Mech. Eng. Part A J. Power Energy* **2003**, *217*, 413–419. [CrossRef]
29. McAuliffe, B.R.; Yaras, M.I. Numerical study of instability mechanisms leading to transition in separation bubbles. *ASME J. Turbomach.* **2008**, *130*, 021006. [CrossRef]